# Combustion in miscible displacement for high-pressure air injection

Gargar, N. Khoshnevis; Bruining, J.; Kokubun, M. A.Endo; Marchesin, D.; Mailybaev, A. A.

**DOI**
10.1007/s10596-020-09977-y

**Publication date**
2020

**Document Version**
Final published version

**Published in**
Computational Geosciences

**Citation (APA)**
Gargar, N. K., Bruining, J., Kokubun, M. A. E., Marchesin, D., & Mailybaev, A. A. (2020). Combustion in miscible displacement for high-pressure air injection. *Computational Geosciences*, *24*(4), 1663-1672. https://doi.org/10.1007/s10596-020-09977-y

Computational Geosciences (2020) 24:1663–1672
https://doi.org/10.1007/s10596-020-09977-y

ORIGINAL PAPER

# Combustion in miscible displacement for high-pressure air injection

N. Khoshnevis Gargar[1] · J. Bruining[2] · M. A. Endo Kokubun[3] · D. Marchesin[4] · A. A. Mailybaev[4]

Received: 19 October 2018 / Accepted: 19 May 2020 / Published online: 5 June 2020


**Abstract**

This paper describes miscible displacement upon air injection in a porous medium saturated with oil corresponding to conditions of high-pressure air injection (HPAI). We assume that injection fluids and produced fluids are fully miscible with the oil at the prevailing high pressure. We use three pseudo-components, viz., oxygen, oil, and an inert component, which includes nitrogen, carbon dioxide, etc. To model the fingering instabilities, we follow a similar procedure as proposed by Koval (SPE J. **3**(02):145–154, 1963) and include the reaction between oxygen and oil in the Koval model. The equations are solved numerically, using a finite element software package (COMSOL). The results show that a combustion wave is formed. We study the performance at low and high viscosities and show that the reaction improves the speed and degree of recovery at later times.

**Keywords** High-pressure air injection · In-situ combustion · Koval model · Miscible displacement · Porous media

## 1 Introduction

There is a large body of literature describing the use of high-pressure air injection (HPAI) to recover oil [3, 8, 10, 15, 21, 22]. Application of HPAI, above 100 bars, is confined to reservoirs at large depths. Its effectiveness depends on the prevailing conditions [9] including the displacement efficiency and the areal and vertical sweep efficiency, oil swelling, oil viscosity reduction, and thermal effects due to the oxidation reactions. An improved understanding of the HPAI process is required in order to prevent the oxygen from reaching the production wells, which is considered a safety hazard [14].

We consider a miscible HPAI process aimed to enhance recovery of light oil, where in situ combustion and (flue) gas miscible flooding are the main mechanisms depending on gas miscibility and depth of the reservoir [1, 11, 24, 27]. Miscible displacement suffers from a poor areal sweep efficiency and fingering because some factors such as longitudinal dispersion (microscopic heterogeneity), channeling (macroscopic heterogeneity), viscosity (injection of a less viscous solvent), and gravity differences (less dense solvent override) affect the instability of the process at reservoir conditions.

The Koval model [17] considers miscible displacement as if it was an immiscible displacement process where a solvent phase is "diluted" with the initial oil at a proportion of 78% oil and 22% solvent. The viscosity for the mixture can be calculated by the fourth root mixing rule. The relative permeabilities are taken as being proportional to the respective saturations of the phases. This model has been proven to be able to describe viscous fingering at a macroscopic level as confirmed experimentally [4].

The objective of this paper is to develop a model for the reactive miscible displacement of oil by air injection and to show that such mechanism can enhance recovery. Our special focus will be on the inclusion of the effect of fingering using the Koval procedure, which shares some similarities with the Buckley–Leverett model. Our basic assumptions in this model are summarized as the system is one dimensional and the injected air is miscible with oil in the first contact at all proportions, as expected at high pressure. The fluids are assumed to be ideal; therefore, there will be no heat and volume effects upon mixing. The

✉ N. Khoshnevis Gargar
Negar.khoshnevisgargar@deltares.nl

1 Deltares, Unit Geo-Engineering, Boussinesqweg 1, 2629 HV Delft, The Netherlands

2 Civil Engineering and Geosciences, Delft University of Technology, Delft, The Netherlands

3 Department of Chemistry, University of Bergen, Bergen, Norway

4 Instituto Nacional de Matemática Pura e Aplicada –IMPA, Rio de Janeiro, Brazil

injected oxygen in the air stream reacts with oil, generating a heat wave. The numerical solution provides the average concentrations of oil, oxygen, and inert components as functions of distance and time, where the inert component includes all combustion products.

The structure of the paper is as follows. First, we describe the physical model and present the governing equations. Next, we give a theoretical description of waves that appear in the solution. Afterwards, we introduce empirical parameters into the model to take into account the fingering behavior and perform numerical simulations for different reservoir conditions. We also perform $2D$ simulations to show, qualitatively, that the Koval model describes well the macroscopic behavior. Finally, we draw the main conclusions of this study.

## 2 Modeling HPAI with the Koval model

Our interest is in considering the case when the injected and produced gases become completely miscible with the oil at sufficiently high pressures. This occurs, e.g., when the injected fluid forms a developed miscible process. In this process, the methane dissolved in the oil helps to develop a methane bank, which is miscible with the injected air on the trailing side and miscible with the oil to be recovered on the leading side [26].

We study a 1D flow problem involving a miscible flow when air is injected into porous rock filled with oil at high pressures. The injected fluid (air) consists of oxygen and inert components. A simple model includes three pseudo-components characterizing oil, oxygen, and inert component. The respective volumetric fractions are denoted by $c_{oil}$, $c_{ox}$, and $c_{in}$ with the unit sum, $c_{oil} + c_{ox} + c_{in} = 1$.

### 2.1 Koval model

The Koval model [17] considers miscible displacement characterized by fingering of the solvent into the oil, as if there are two phases. The first phase is a solvent, which contains air and reaction products with the saturation $c_s = c_{ox} + c_{in}$. The second phase is the initial oil, which has saturation $c_{oil} = 1 - c_s$. To incorporate the miscibility in 1D displacement process, it was proposed to use linear relative permeabilities proportional to the respective saturations. The fractional-flow function in the Buckley–Leverett equation for the solvent is therefore replaced by

$$f_s(c_s, T) = \frac{c_s/\mu_{\text{mix}}}{c_s/\mu_{\text{mix}} + c_{\text{oil}}/\mu_{\text{oil}}}, \tag{1}$$

where $\mu_{\text{oil}}(T)$ is the oil viscosity and $\mu_{\text{mix}}(T)$ is the specially chosen (effective) solvent phase viscosity dependent on the temperature $T$ (see Eq. 26). Taking $c_{\text{oil}} = 1 - c_s$, Eq. 1 is rearranged as

$$f_s(c_s, T) = \frac{K c_s}{1 + c_s(K-1)}, \tag{2}$$

where $K(T) = HE$ is the Koval factor. This factor is defined as the viscosity ratio $E(T) = \mu_{\text{oil}}/\mu_{\text{mix}}$ multiplied by an experimentally determined heterogeneity factor $H$ [4, 5, 17]. The latter accounts for the higher mobility ratio due to reservoir heterogeneity and can be related to the Dykstra–Parsons' coefficient $V_{DP}$.

From the experimental data [4], it was found that a reasonable effective viscosity of the displacing solvent phase corresponds to the mixture of 78% oil and 22% air [17]. The solvent viscosity can be calculated by the fourth root mixing rule

$$\mu_{\text{mix}}^{-1/4} = 0.78\,\mu_{\text{oil}}^{-1/4} + 0.22\,\mu_{\text{air}}^{-1/4}, \tag{3}$$

where $\mu_{\text{air}}(T)$ is the viscosity of the mixture of oxygen and inert components assumed to be independent of a composition. We refer to the original work by Koval [17] and the thesis of Booth [6] for further details.

### 2.2 Governing equations

The oil reacts with oxygen. It is convenient to include reaction products into the inert pseudo-component and, therefore, to model the reaction as

$$\nu_{\text{oil}}\,[\text{oil}] + \nu_{\text{ox}}\,[O_2] \rightarrow \nu_{\text{in}}\,[\text{inert components}], \tag{4}$$

with the corresponding stoichiometric coefficients. Denoting the reaction rate by $R$, the modified Buckley–Leverett equation for the reacting solvent reads

$$\varphi \frac{\partial c_s}{\partial t} + \frac{\partial}{\partial x}(u f_s) = (\nu_{\text{in}} - \nu_{\text{ox}})R, \tag{5}$$

where $\varphi$ is the porosity and the fractional-flow function is given in Eq. 2. The analogous equation for the oil phase has the form

$$\varphi \frac{\partial c_{\text{oil}}}{\partial t} + \frac{\partial}{\partial x}(u f_{\text{oil}}) = -\nu_{\text{oil}} R, \quad f_{\text{oil}} = 1 - f_s. \tag{6}$$

Summing the two Eqs. 5 and 6 and using the conditions $c_s + c_{\text{oil}} = 1$ and $f_s + f_{\text{oil}} = 1$ yields the equation determining the Darcy velocity as

$$\frac{\partial u}{\partial x} = (\nu_{\text{in}} - \nu_{\text{ox}} - \nu_{\text{oil}})R. \tag{7}$$

We will also need the balance law determining the oxygen fraction $c_{\text{ox}}$, which is a part of the solvent phase. It reads

$$\varphi \frac{\partial c_{\text{ox}}}{\partial t} + \frac{\partial}{\partial x}(u f_{\text{ox}}) = -\nu_{\text{ox}} R, \quad f_{\text{ox}} = \frac{c_{\text{ox}}}{c_s} f_s. \tag{8}$$

The fraction of inert components is expressed by $c_{\text{in}} = 1 - c_{\text{oil}} - c_{\text{ox}}$. In writing (5–8), we disregarded molecular diffusion and dispersion.

Assuming that the temperature of solid rock, liquid, and gas are equal, we write the heat balance equation as

$$\frac{\partial}{\partial t}(C_m \Delta T + \varphi C_o \Delta T) + \frac{\partial}{\partial x}(C_o u \Delta T) = \lambda \frac{\partial^2 T}{\partial x^2} + QR, \quad (9)$$

where $\Delta T = T - T_{ini}$ is the temperature relative to the initial reservoir, $\lambda$ is the thermal conductivity, $Q$ is the heat of the combustion reaction, and $C_m$ is the rock matrix heat capacity. The volumetric heat capacity of liquids is approximately $C_o \approx 2 \times 10^6$ J/m$^3$/K, and therefore, we assume that it can be taken independent of composition. We disregard any volume change due to reactions, temperature expansion, and compositional mixing. The pressure drop is considered to be small with respect to the prevailing pressure $P$ and is therefore disregarded.

We consider the reaction rate as

$$R = \varphi A_r c_{\text{oil}} c_{\text{ox}}^n \exp\left(-\frac{T_{\text{ac}}}{T}\right), \quad (10)$$

where $A_r$ is the frequency factor for the oxidation rate of oil and $n$ is the order of reaction with respect to oxygen. We use $T_{\text{ac}}$ to denote the activation temperature for the oxidation rate. The activation temperature is related to the activation energy $E_{\text{ac}}$ by $T_{\text{ac}} = E_{\text{ac}}/R$.

### 2.3 Initial and boundary conditions

The initial reservoir is saturated with oil at temperature $T_{\text{ini}}$. Thus, we choose the initial conditions as

$$t = 0,\ x \geq 0: \quad c_{\text{oil}} = 1,\ \ c_{\text{ox}} = 0,\ \ T = T_{\text{ini}}. \quad (11)$$

At the injection side, $x = 0$, the air injection boundary conditions are

$$x = 0,\ t \geq 0: \ \ c_{\text{oil}} = 0,\ \ c_{\text{ox}} = c_{\text{ox}}^{\text{inj}},\ \ T = T_{\text{ini}},\ \ u = u^{\text{inj}}. \quad (12)$$

The oxygen fraction in the injected air is $c_{\text{ox}}^{\text{inj}} = 0.21$.

### 2.4 Dimensionless equations

The governing system includes Eqs. 5, 7, 8, and 9. In order to render these equations dimensionless, we introduce the ratios

$$\tilde{t} = \frac{t}{t^*}, \quad \tilde{x} = \frac{x}{x^*}, \quad \theta = \frac{T - T_{\text{ini}}}{\Delta T^*}, \quad \tilde{u} = \frac{u}{\varphi v^*}, \quad (13)$$

where the characteristic values are given by

$$t^* = !\frac{x^*}{v^*}, \quad x^* = \frac{\lambda}{C_m v^*}, \quad v^* = \frac{Q u^{\text{inj}}}{C_m \Delta T^*}, \quad \Delta T^* = T^* - T_{\text{ini}}, \quad (14)$$

and $T^*$ is some characteristic temperature.

We also introduce the following dimensionless parameters

$$\alpha_o = \frac{\varphi C_o}{C_m}, \quad \sigma = \frac{\varphi v^*}{u^{\text{inj}}}. \quad (15)$$

As a result, we obtain the following set of dimensionless equations (we drop the tildes for simplicity)

$$\frac{\partial c_s}{\partial t} + \frac{\partial u f_s}{\partial x} = (\nu_{\text{in}} - \nu_{\text{ox}})r, \quad (16)$$

$$\frac{\partial c_{\text{ox}}}{\partial t} + \frac{\partial u f_{\text{ox}}}{\partial x} = -\nu_{\text{ox}} r, \quad (17)$$

$$\frac{\partial u}{\partial x} = (\nu_{\text{in}} - \nu_{\text{ox}} - \nu_{\text{oil}})r, \quad (18)$$

$$\frac{\partial}{\partial t}(1 + \alpha_o)\theta + \frac{\partial}{\partial x}\alpha_o u \theta = \frac{\partial^2 \theta}{\partial x^2} + \sigma r, \quad (19)$$

where the dimensionless reaction rate is $r = t^* R/\varphi$. The initial and boundary conditions (11) and (12) remain the same except for the last relation $u = u^{inj}$, which takes the dimensionless form $u = 1/\sigma$.

## 3 Solution as a wave sequence

We seek a solution in terms of a series of traveling waves. In analogy with the in situ combustion for lower pressures, which is represented by a multi-phase flow model [2, 12, 13,

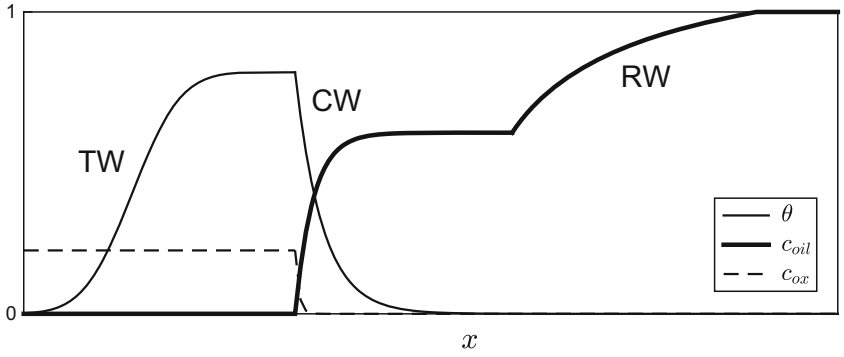


**Fig. 1** Wave sequence solution: the slower thermal wave (TW), the intermediate combustion wave (CW), and the faster rarefaction wave (RW). The dimensionless temperature $\theta$, oil fraction $c_{\text{oil}}$, and oxygen fraction $c_{\text{ox}}$ are shown

16, 18, 19], we assume that a combustion wave is developed along with two additional waves: a slower thermal wave upstream and a faster Buckley–Leverett (rarefaction or shock) wave downstream, shown schematically in Fig. 1. Such wave solution is asymptotic, i.e., it develops at sufficiently large times (and sufficiently long distances) after the initial transient behavior.

In this section, we show that the faster wave located downstream is a rarefaction wave that occurs due to mixing between oil and inert miscible components. The slower wave, located upstream, is the thermal wave, where only the injected air (with no oil) is present. These two waves allow analytical description presented below.

In between, there is a combustion wave, where reaction between oxygen and oil takes place. So far, no analytical theory is developed for the combustion wave in the fully miscible HPAI process. This combustion wave will be studied numerically in the next section, and we expect that these results facilitate future theoretical developments.

### 3.1 Thermal wave

In the thermal wave, upstream, no reaction takes place, i.e., $r = 0$; Fig. 1. Therefore, the energy equation is given by

$$(1+\alpha_o)\frac{\partial}{\partial t}\theta + \alpha_o \frac{\partial}{\partial x} u\theta = \frac{\partial^2 \theta}{\partial x^2}. \tag{20}$$

The total mass conservation (18) with the injection boundary condition $u = 1/\sigma$ yields the constant velocity $u \equiv 1/\sigma$ within the whole thermal wave. Therefore, we have the following equation valid for the thermal wave

$$\frac{\partial \theta}{\partial t} + \frac{\alpha_o}{\sigma(1+\alpha_o)}\frac{\partial \theta}{\partial x} = \frac{1}{(1+\alpha_o)}\frac{\partial^2 \theta}{\partial x^2}. \tag{21}$$

This equation has a well-known solution (see, e.g., [7])

$$\theta(x,t) = \theta_h \left( \frac{1}{2} + \frac{1}{2}\,\mathrm{erf}\left[ \frac{x - x_T - v_T t}{2\sqrt{t/(1+\alpha_o)}} \right] \right), \tag{22}$$

where $v_T = \alpha_o/(\sigma(1+\alpha_o))$ is the wave speed, $x_T$ is an arbitrary number specifying the wave position, and $\mathrm{erf}(x)$ is the error function. We conclude that the thermal wave travels with the constant speed $v_T$, while its width increases with a rate proportional to $\sqrt{t/(1+\alpha_o)}$.

### 3.2 Rarefaction wave

In the region downstream of the combustion wave, the reservoir has constant temperature equal to the initial value, $\theta = 0$. Also, no oxygen is present, $c_{\mathrm{ox}} = 0$, which means that the flow is nonreactive, $r = 0$. Therefore, the flow represents the miscible displacement at constant temperature with just two components: the oil with fraction $c_{oil}$ and the remaining inert components with $c_s = c_{in} = 1 - c_{oil}$. The Darcy velocity given by Eq. 18 is constant in this region, $u \equiv u_r$. In general, the value $u_r$ may be different from the injection velocity due to the reaction in the combustion wave upstream.

The dynamics is governed by the equation following from Eqs. 2 and 16 as

$$\frac{\partial c_s}{\partial t} + u_r \frac{\partial f_s}{\partial x} = 0, \quad f_s(c_s) = \frac{K_0 c_s}{1 + c_s(K_0 - 1)}, \tag{23}$$

with the Koval factor $K_0$ computed at $\theta = 0$. Equation 23 is the classical Buckley–Leverett equation [25] (see also [6] for its application to miscible flows).

In the case of practical interest, we have $\mu_{\mathrm{oil}} > \mu_{\mathrm{mix}}$ and, therefore, $K_0 > 1$. One can verify that the function $f_s(c_s)$ in Eq. 23 is concave, i.e., $d^2 f_s/dc_s^2 < 0$. The solvent fraction $c_s$ must decrease in downstream direction from some positive value to zero (initial reservoir is filled by oil). Under such conditions, solution of Eq. 23 represents a self-similar rarefaction wave of the form [25]

$$c_s(x,t) = F(\xi), \quad c_{\mathrm{oil}}(x,t) = 1 - F(\xi), \quad \xi = \frac{x}{t}, \tag{24}$$

where $F(\xi)$ is the function to be determined and $\xi$ changes in some finite interval. After substituting (24) into (23) and dropping the common factor $F'$, elementary manipulations yield

$$F(\xi) = \frac{\sqrt{K_0 u_r/\xi} - 1}{K_0 - 1}. \tag{25}$$

Expressions (24) and (25) describe the rarefaction wave solution explicitly. This solution is determined in the interval $\xi_1 \le \xi \le \xi_2$. The downstream limit is obtained from the condition that $c_s = 0$, which yields $\xi_2 = K_0 u_r$. The upstream limit $\xi_1$ can be obtained similarly if the corresponding fraction of the solvent is known.

## 4 Numerical modeling

We consider a fully coupled, implicit numerical solution approach based on finite-elements, which is solved with the COMSOL software. We apply the mathematical module of COMSOL to introduce the model equations in weak form.

We consider the spatial domain $0 \le x \le L$ of length $L = 50$ m, where the Neumann boundary condition is taken at the production side, $x = L$ for the modified Buckley–Leverett equation. The grid size in the numerical simulation is 0.01 m, which corresponds to 5000 grid cells. This is fine enough to capture the multi-scale processes and is capable of resolving the salient features.

We consider reservoir parameter values given in Table 1. Parameters of the reaction rate vary considerably depending on specific conditions, but the availability of reaction rate data is limited. Our choice corresponds to heptane ($C_7H_{16}$)

**Table 1** Values of reservoir parameters for heptane as a model oil

| | | |
|---|---|---|
| $A_r$ | 4060 1/s | frequency factor for the reaction |
| $C_m$ | 2 MJ/m $^3$K | rock matrix heat capacity |
| $C_o$ | 1.5 MJ/m$^3$K | volumetric heat capacity of liquids |
| $H$ | 1 | heterogeneity factor |
| $n$ | 1 | order of reaction |
| $Q$ | 440 kJ/mol | heat of combustion reaction |
| $T_{\text{ac}}$ | 7066 K | activation temperature |
| $T_{\text{ini}}$ | 300 K | initial reservoir temperature |
| $u^{\text{inj}}$ | $8.0 \times 10^{-7}$ m/s | injection Darcy velocity |
| $\lambda$ | 3 W/m K | thermal conductivity |
| $\nu_{\text{oil}}$ | 0.090 [mol/mol] | stoichiometric coefficient for oil |
| $\nu_{\text{ox}}$ | 1 [mol/mol] | stoichiometric coefficient for oxygen |
| $\nu_{\text{in}}$ | 1.36 [mol/mol] | stoichiometric coefficient for reaction products |
| $\varphi$ | 0.3 | porosity |

as a combustion fuel [12, 13, 20]. For the viscosities (in cP with $T$ in K), we use

$$\mu_{\text{oil}}(T) = \exp\left(\frac{1335.8}{T} - 4.6329\right), \quad \mu_{\text{air}}(T) = \frac{7.5}{T+120}\left(\frac{T}{291}\right)^{3/2}. \tag{26}$$

viz., Sutherland's formula for the gas (air) viscosity and the Arrhenius model for liquid viscosities [23].

Expressions (26) define the viscosity of the base case for our numerical simulations. The other cases correspond to the oil of high viscosity (ten times the base case) and low viscosity (one-third of the base case).

## 4.1 Base case

Numerical results for the base case are shown in Fig. 2. Here, the numerical solution features three different waves: thermal, combustion, and rarefaction. The thermal wave, which has been described theoretically in Section 3.1, corresponds to the rise of temperature $T$ without changing the flow composition as can be seen in the interval between $0 - 7$ m in the left and between $0 - 15$ m in the right panel of Fig. 2. The thermal wave is the slowest one, and it travels in the section of the reservoir where the oil is already displaced, $c_{\text{oil}} = 0$, and the miscible phase is composed of the injected oxygen and inert components whose fractions are constant and equal to their values at the injection side along the thermal wave. The temperature changes from the initial value $T = T_{\text{ini}}$ to some larger value in the plateau.

At $x = 8$ m in the left and $x = 31$ m in the right of Fig. 2, the reaction between oxygen and oil in a single miscible phase creates the combustion wave. The injected oxygen is consumed completely in this region, leading to a sharp peak of the inert component concentration. No reaction occurs in the plateau downstream of this wave, where the oxygen fraction $c_{\text{ox}}$ is zero. The oil fraction downstream of the combustion wave is $c_{\text{oil}} \approx 0.7$. This value characterizes the constant oil flux between the combustion wave and the rarefaction wave downstream. Since no oil is left upstream of the combustion wave, one can attribute $c_{\text{oil}} \approx 0.7$ to the inert components fraction $c_{\text{in}}$. In the solution profiles, one observes the formation of thermal, combustion, and rarefaction waves

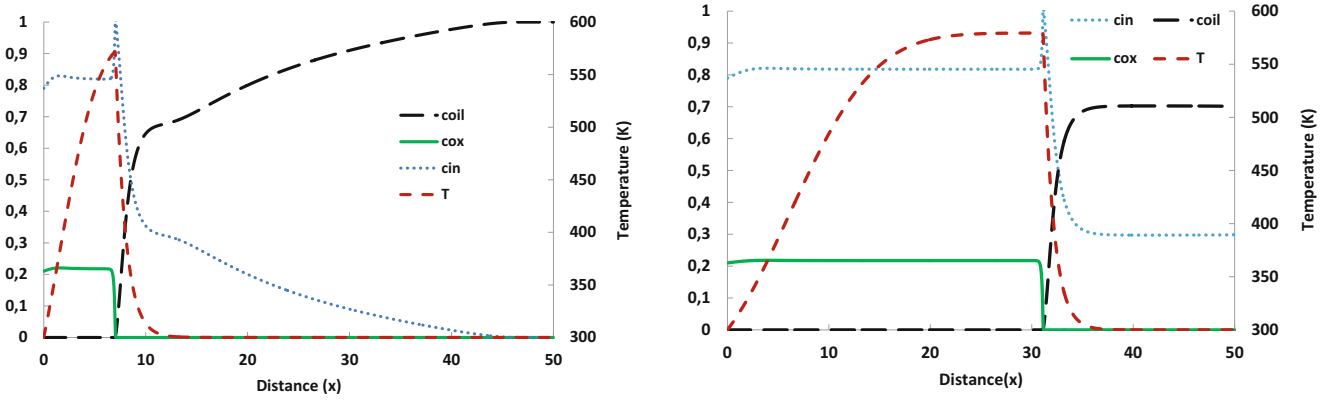


**Fig. 2** Simulation of HPAI into a porous media filled with oil. The left panel corresponds to the time $t = 5 \times 10^6$ s, and the right panel to $t = 2 \times 10^7$ s. Left y-axis shows the fraction. Indicated are the distributions of the temperature $T$, oil fraction $c_{\text{oil}}$, oxygen fraction $c_{\text{ox}}$, and

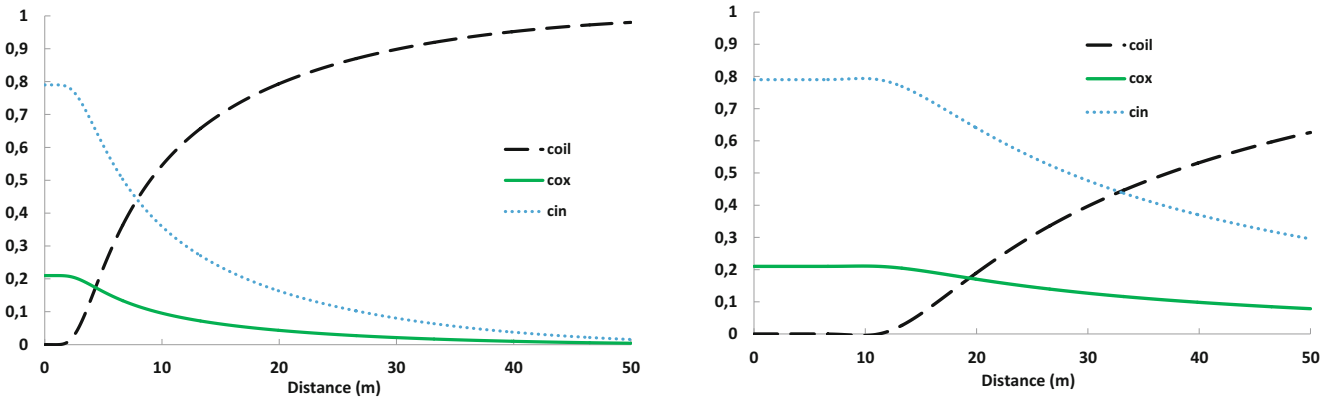


**Fig. 3** Simulation for HPAI into a porous media filled with oil when the reaction is not present. Same variables are shown at the same times as in Fig. 2. Left y-axis shows the fraction

fraction of oil produced via the combustion wave (see also Fig. 9 below).

Downstream of the combustion wave, there is a rarefaction wave. As described in Section 3.2, the rarefaction wave features the miscible displacement of inert components and oil at the constant temperature (see the left figure of Fig. 2) in the region of $14-45$ m (in the right panel, the rarefaction wave already has left the simulation domain). This wave is the fastest one and responsible for the initial oil recovery. In the rarefaction region, temperature has its initial value of $T = T_{\text{ini}}$ and no reaction occurs.

We used the same parameters for another simulation of miscible gas injection, where no reaction was present. The results have been shown in Fig. 3 at two different times, $t = 5 \times 10^6$ s and $t = 2 \times 10^7$ s. In this case, there is no thermal and combustion waves as there are no reaction involved in the process. The only present wave is the rarefaction wave, which is responsible for oil recovery. The shape of this wave is due to the Koval model equations. The oxygen and inert components decrease gradually from their injected upstream values to zero downstream, while the miscible air is pushing the oil out. The corresponding gradual increase of oil recovery will be shown in Fig. 9 below, which is less efficient than the reactive recovery at later times.

## 4.2 Effect of viscosity

In this section, we study the effect of the viscosity on the wave structure in the high-pressure miscible air injection process. We consider two different situations: a high oil viscosity (ten times the base case) and a low oil viscosity (one-third of the base case). The numerical results are shown in Fig. 4 for higher viscosity oil and in Fig. 5 for lower viscosity oil at the same times as in the base case. One observes that the sequence of waves is preserved. In Fig. 4, the temperature ($T \approx 850$ K) is higher than the base case due to the slow movement of the fuel leading to combustion. The left panel in Fig. 4 reveals that a smaller amount of oil ($\Delta c_{\text{oil}} \approx 0.2$) is attributed to miscible displacement in a rarefaction wave, while a big bank of the oil with $c_{\text{oil}} \approx 0.8$ is located downstream of the combustion wave. This behavior will also be confirmed by the recovery factors shown in Fig. 9 below.

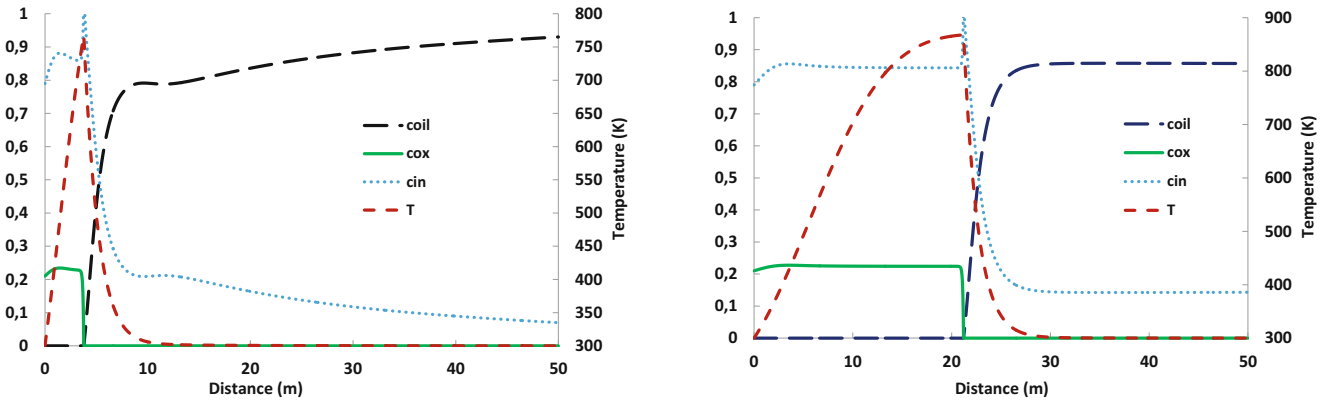


**Fig. 4** Simulation for HPAI into a porous media filled with oil of higher viscosity. Same variables are shown at the same times as in Fig. 2. Left y-axis shows the fraction

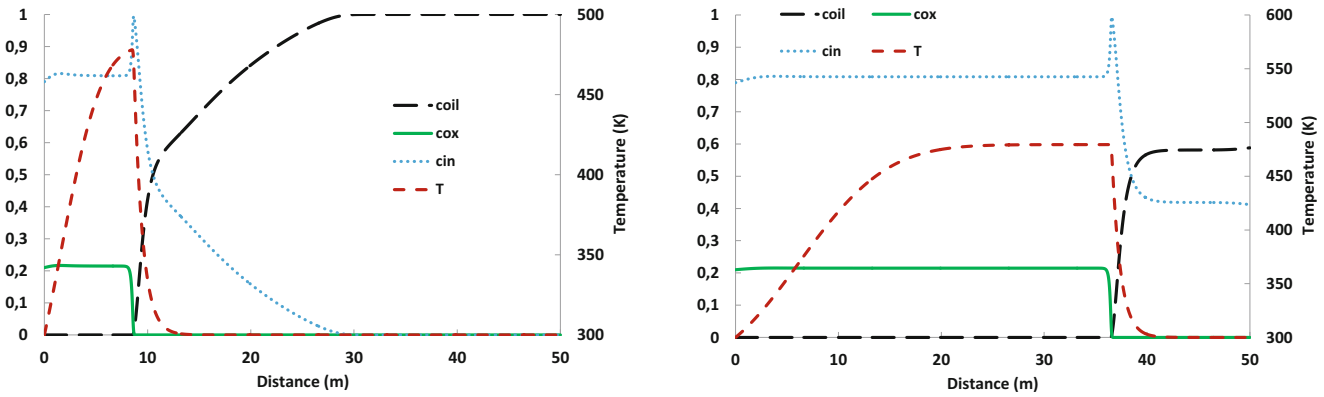


**Fig. 5** Simulation for HPAI into a porous media filled with oil of lower viscosity. Same variables are shown at the same times as in Fig. 2. Left y-axis shows the fraction

Similar wave sequences are shown in Fig. 5 for the simulation with a lower viscosity oil. Now, a considerably larger fraction of the oil is produced by miscible gas flooding in the rarefaction wave ($\Delta c_{\text{oil}} \approx 0.45$). The combustion wave is responsible for the occurrence of an oil bank located downstream of the combustion wave with $c_{\text{oil}} \approx 0.55$. The highest temperature in this case is $T \approx 480$ K, which is lower than in the base case due to the higher velocity of the combustion wave. In all the cases, no oil is left upstream of the combustion and rarefaction waves, leading to the complete recovery.

As shown in Fig. 4 (left panel), the breakthrough of miscible inert components at the production side occurs at earlier times, compared to the breakthrough for both the base case in Fig. 2 and the lower viscosity oil in Fig. 5.

### 4.3 Two-dimensional numerical simulation

In this section, we consider a 2D numerical simulation approach to model the miscible air injection. The model includes three components characterizing oil, oxygen, and inert compounds. We consider miscible phase which contains oxygen, oil, and reaction products with the saturation of $c_{\text{ox}}$, $c_{\text{oil}}$, and $c_{\text{in}}$. In this section, we have not applied Koval method. Therefore, we test basic assumptions of the Koval method by the direct observationof fingering instabilities in the combustion process. The set of governing equations are given by

$$\varphi \frac{\partial c_{\text{oil}}}{\partial t} + \nabla \cdot (u c_{\text{oil}} - \varphi D_{\text{oil}} \nabla c_{\text{oil}}) = -\nu_{\text{oil}} R, \quad (27)$$

$$\varphi \frac{\partial c_{\text{ox}}}{\partial t} + \nabla \cdot (u c_{\text{ox}} - \varphi D_{\text{ox}} \nabla c_{\text{ox}}) = -R, \quad (28)$$

$$\varphi \frac{\partial c_{\text{in}}}{\partial t} + \nabla \cdot (u c_{\text{in}} - \varphi D_{\text{in}} \nabla c_{\text{in}}) = \nu_{\text{in}} R, \quad (29)$$

$$\nabla \cdot u = (\nu_{\text{in}} - \nu_{\text{oil}} - 1) R, \quad (30)$$

$$(C_m + \varphi C_o) \frac{\partial T}{\partial t} + \nabla \cdot (C_o u T) = \nabla \cdot (\lambda \nabla T) + Q R. \quad (31)$$

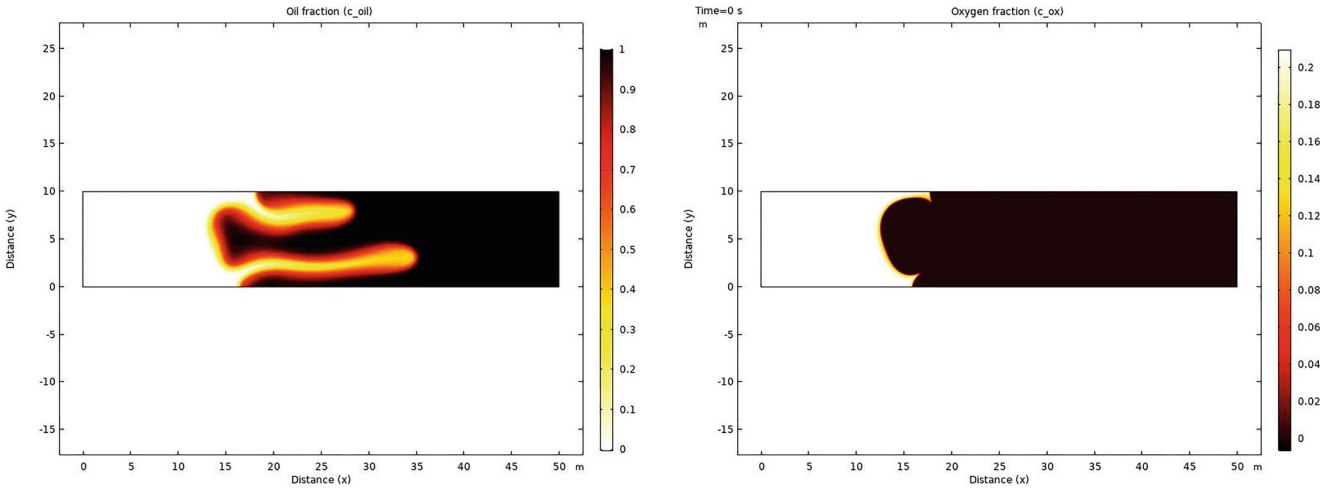


**Fig. 6** 2D simulation for HPAI into a porous media filled with oil. Indicated by color are the distribution of oil fraction $c_{\text{oil}}$ (left) and oxygen fraction $c_{\text{ox}}$ (right)

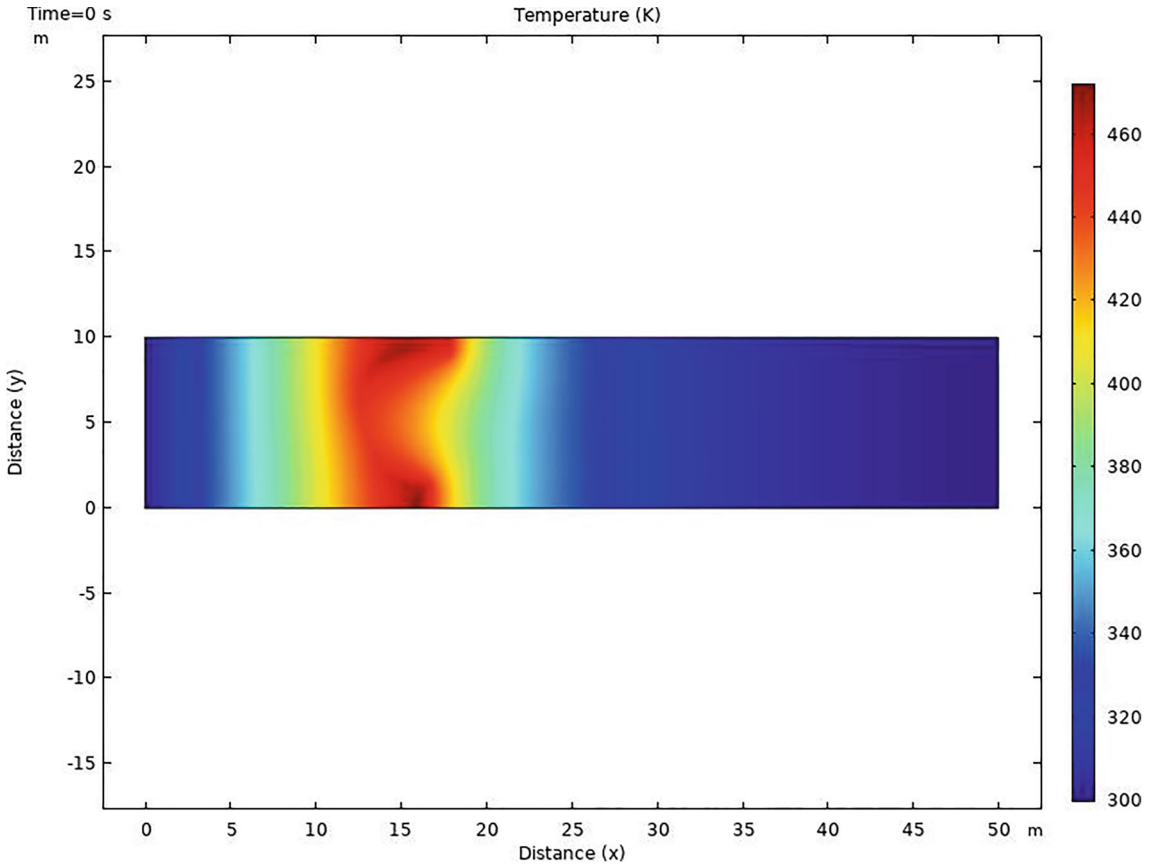


**Fig. 7** 2D simulation for HPAI into a porous media filled with oil. Indicated by color is the temperature $T$

Equation 30 determines the pressure field through Darcy's law

$$u = -\frac{K}{\mu_{\text{mix}}}\nabla p. \tag{32}$$

The parameters are given by

$$\mu_{\text{oil}} = \exp\left(\frac{1335.8}{T} - 4.6329\right), \quad \mu_{\text{ox}} = \mu_{\text{in}} = \frac{7.5}{T+120}\left(\frac{T}{291}\right)^{3/2}, \tag{33}$$

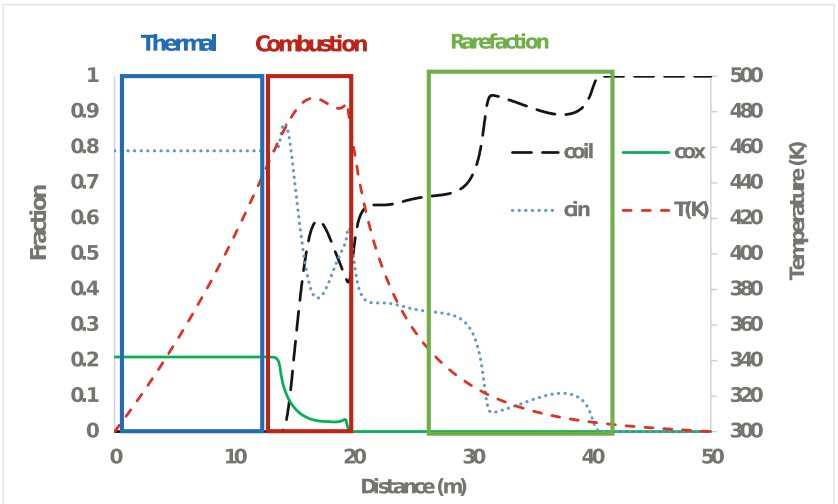


**Fig. 8** Oil, oxygen, and inert products fractions and temperature profiles of 2D simulation, averaged in the direction $y$ transverse to the flow. One can qualitatively distinguish the regions that can be attributed to the thermal, combustion, and rarefaction waves

$$\frac{1}{\mu_{\text{mix}}^{1/4}} = \frac{c_{\text{oil}}}{\mu_{\text{oil}}^{1/4}} + \frac{c_{\text{ox}}}{\mu_{\text{ox}}^{1/4}} + \frac{c_{\text{in}}}{\mu_{\text{in}}^{1/4}}. \tag{34}$$

Due to limitation caused by instabilities in numerical scheme, the simulation is performed with increased values of diffusion coefficients $D_{\text{oil}} = D_{\text{ox}} = D_{\text{in}} = 0.5 \times 10^{-9}$ m$^2$/s. The reaction is given by

$$R = \varphi A_r \rho c_{\text{oil}} c_{\text{ox}} \left(\frac{P_0}{P_{\text{atm}}}\right)^n \exp\left(-\frac{T_{\text{ac}}}{T}\right), \tag{35}$$

whereas the initial conditions are given by

$$t = 0, x \geq 0: \quad T = 300\ K, \quad c_{\text{oil}} = 1, \quad c_{\text{ox}} = c_{\text{in}} = 0, \quad p = 10^6\ Pa \tag{36}$$

and the boundary conditions by

$$t > 0, x = 0: \quad T = 300\ K, \quad c_{\text{oil}} = 0, \quad c_{\text{ox}} = 0.21, \quad c_{\text{in}} = 0.79, \quad p = 1.01 \times 10^6\ Pa \tag{37}$$

For the upper $y = 10$ m and lower $y = 0$ m part of the domain, we consider no flux boundary conditions for all variables. 2D numerical simulation results are shown in Figs. 6 and 7. The 2D results show the fingering of the miscible reaction products into the oil. As a result, a mixture of the oil and inert products travels downstream the combustion front. The profiles of all components and temperature, averaged in the transverse $y$-direction, are presented in Fig. 8. Three different regions can be distinguished, which correspond to the thermal wave (large temperature increase at no change in saturations), the combustion wave (full oxygen consumption) and, after a short nearly constant state the rarefaction wave (change of saturations at low temperatures).

The performed 2D simulation captures the formation of just two fingers, which makes it under-resolved for a detailed quantitative comparison with the Koval approximation. Certainly, both a considerable increase in the physical domain and a more detailed statistical analysis are necessary, and we leave this nontrivial numerical problem for future work. Still, from the performed simulation, one can conclude that satisfactory qualitative agreement is demonstrated with the results of the previous sections, therefore, suggesting that both 2D physical model and Koval model are capable of capturing viscous fingering on a macroscopic level including reaction.

### 4.4 Efficiency of the combustion wave and miscible gas flooding

The amount of oil recovered relative to the amount of initial oil in place (recovery factor) versus time is shown in Fig. 9 for all cases, i.e., the base case, with and without reaction, and for oils with higher or lower viscosities. One can clearly distinguish two stages of the recovery history. The first stage is characterized by approximately constant recovery rates (slopes). The recovery mechanism is controlled by the rarefaction wave (miscible gas flow), which reaches the production side in about 100−170 days. The reservoir states corresponding to this early stage are presented in the left figures of all cases in Figs. 2–5. This initial recovery is not affected by thermal effects, because the temperature is

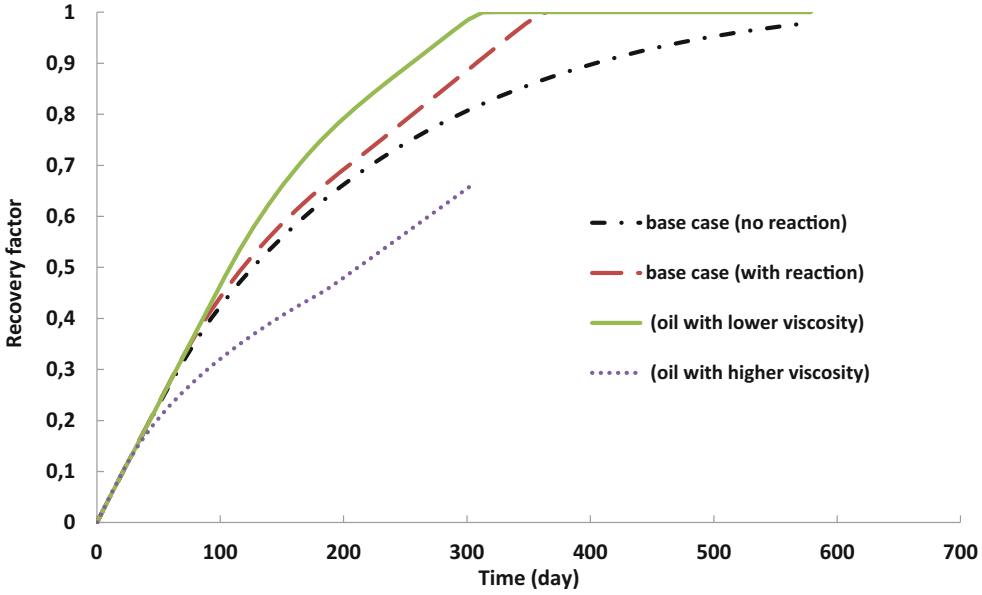


**Fig. 9** Recovery factors obtained by simulations for HPAI for different oil viscosities. One of the curves (base case (no reaction)) demonstrates the results when the reaction is not included in the model

constant along the rarefaction wave. The second recovery stage is less steep and it is controlled by the combustion wave. In this process, the recovery factor increases until it reaches the maximum value of 1 corresponding to the complete oil recovery. In the case of no reaction, the process is controlled by the rarefaction wave at all times. In this case, the recovery process is much less efficient at later times, when the growth of the recovery factor is hampered.

## 5 Conclusions

It is possible to use Koval's theory to study miscible displacement including combustion of oil for high-pressure conditions (HPAI) using a simplified model that considers only three components, viz. oxygen, oil, and an inert component that includes nitrogen, carbon dioxide, etc. The model is capable of grasping viscous instabilities (fingering) on a macroscopic level and to include the reaction between oxygen and oil. The equations can be solved numerically, using a finite element software package (COMSOL). The results show that a combustion wave is formed both for high and low viscosity oil. Moreover, it is shown that the reaction improves the speed and degree of recovery, which attains values of 100% in a reasonable time after 1.4 PV air injected.

**Funding information** This work was supported by the CNPq (grants 303047/2018-6, 406431/2018-3) and the Program FAPERJ Pensa Rio (grant E-26/210.874/2014).

## References

1. Adetunji, L., Teigland, R.: Light-oil air-injection performance: sensitivity to critical parameters. In: SPE Annual Technical Conference and Exhibition, volume SPE 96844 (2005)
2. Akkutlu, I.Y., Yortsos, Y.C.: The dynamics of in-situ combustion fronts in porous media. Combust. Flame **134**, 229–247 (2003)
3. Barzin, Y., Moore, R.G., Mehta, S.A., Ursenbach, M.G., Tabasinejad, F.: Effect of interstitial water saturation and air flux on combustion kinetics of high pressure air injection (HPAI). In: SPE Western Regional Meeting, volume SPE 133599 (2010)
4. Blackwell, R.J., Rayne, J.R., Terry, W.M.: Factors influencing the efficiency of miscible displacement. AIME Petroleum Trans. **217**, 1–8 (1959)
5. Blackwell, R.J., Terry, W.M., Rayne, J.R., Lindley, D.C., et al.: Recovery of oil by displacements with water-solvent mixtures. Petroleum Transactions, 219 (1960)
6. Booth, R.J.: Miscible flow through porous media. PhD thesis. University of Oxford (2008)
7. Bruining, J., Mailybaev, A.A., Marchesin, D.: Filtration combustion in wet porous medium. J. SIAM Appl. Math. **70**, 1157–1177 (2009)
8. Chen, Z., Wang, L., Duan, Q., Zhang, L., Ren, S.: High-pressure air injection for improved oil recovery: Low-temperature oxidation models and thermal effect. Energy & Fuels **27**(2), 780–786 (2013)
9. Clara, C., Durandeau, M., Quenault, G., Nguyen, T.H.: Laboratory studies for light-oil air injection projects: potential application in Handil field. SPE Reservoir Eval. Eng. **3**(3), 239–248 (2000)
10. Denney, D.: 30 years of successful high-pressure air injection: Performance evaluation of Buffalo field, South Dakota. J. Petrol. Tech. **63**(01), 50–53 (2011)
11. Fassihi, M.R., Yannimaras, D.V., Westfall, E.E., Gillham, T.H.: Economics of light oil air injection projects. In: SPE/DOE Improved Oil Recovery Symposium, volume SPE 3593-MS (1996)
12. Gargar, N.K., Mailybaev, A.A., Marchesin, D., Bruining, H.: Effects of water on light oil recovery by air injection. Fuel **137**, 200–210 (2014)
13. Gargar, N.K., Mailybaev, A.A., Marchesin, D., Bruining, H.: Diffusive effects on recovery of light oil by medium temperature oxidation. Transp. Porous Media **105**(1), 191–209 (2014)
14. Greaves, M., Ren, S., Rathbone, R., Fishlock, T., Ireland, R.: Improved residual light oil recovery by air injection (LTO process). Journal of Canadian Petroleum Technology, 39(1) (2000)
15. Gutierrez, D., Taylor, A., Kumar, V., Ursenbach, M., Moore, R., Mehta, S.: Recovery factors in high-pressure air injection projects revisited. SPE Reservoir Eval. Eng. **11**(6), 1097–1106 (2008)
16. Endo Kokubun, M.A., Gargar, N.K., Bruinning, H., Mailybaev, A.A.: Multicomponent effects in liquid–gas filtration combustion. Combust. Flame **169**, 51–62 (2016)
17. Koval, E.J.: A method for predicting the performance of unstable miscible displacement in heterogeneous media. SPE J. **3**(02), 145–154 (1963)
18. Mailybaev, A., Bruining, J., Marchesin, D.: Analytical formulas for in-situ combustion. SPE J. **16**(03), 513–523 (2011)
19. Mailybaev, A.A., Marchesin, D., Bruining, J.: Resonance in low-temperature oxidation waves for porous media. SIAM J. Math. Anal. **43**, 2230 (2011)
20. Mailybaev, A.A., Marchesin, D., Bruining, J.: Recovery of light oil by medium temperature oxidation. Transp. Porous Media **97**(3), 317–343 (2013)
21. Montes, A.R., Gutierrez, D., Moore, R.G., Mehta, S.A., Ursenbach, M.G.: Is high-pressure air injection (HPAI) simply a flue-gas flood J. Can. Pet. Technol. **49**(2), 56–63 (2010)
22. Moore, R.G., Mehta, S.A., Ursenbach, M.G.: A guide to high pressure air injection (HPAI) based oil recovery. In: SPE/DOE Improved Oil Recovery Symposium, volume SPE 75207-MS (2002)
23. Poling, B.E., Prausnitz, J.M., O'Connell, J.P.: The Properties of Gases and Liquids. McGraw-Hill, New York (2001)
24. Ren, S.R., Greaves, M., Rathbone, R.R.: Air injection LTO process: an IOR technique for light-oil reservoirs. SPE J. **7**(1), 90–99 (2002)
25. Smoller, J.: Shock Waves and Reaction-Diffusion Equations. Springer, New York (1983)
26. Stalkup, F.I. Jr..: Status of miscible displacement. J. Petrol. Tech. **35**(04), 815–826 (1983)
27. Turta, A.T., Singhal, A.K.: Reservoir engineering aspects of light-oil recovery by air injection. SPE Reserv. Eval. Eng. **4**(4), 336–344 (2001)